HYBRID RANS/PDF CALCULATIONS OF A SWIRLING BLUFF BODY FLAME ('SM1'): INFLUENCE OF THE MIXING MODEL

R. De Meester, B. Naud, U. Maas, B. Merci

Proceedings of MCS 7, Chia Laguna, Cagliari, Sardinia, Italy, September 11-15, 2011

HYBRID RANS/PDF CALCULATIONS OF A SWIRLING BLUFF BODY FLAME ('SM1'): INFLUENCE OF THE MIXING MODEL

R. De Meester[1], B. Naud[2], U. Maas[3], B. Merci[1]
reni.demeester@ugent.be
[1]Ghent University , Department of Flow, Heat and Combustion Mechanics, Ghent, Belgium

[2] Modeling and Numerical Simulation Group, Energy Dept., Ciemat, Madrid, Spain

[3] Institute for Technical Thermodynamics, Karlsruhe University (TH), Karlsruhe, Germany

Abstract

In this work, we perform steady 2D axisymmetric hybrid RANS/PDF calculations of a swirling bluff body flame (SM1), studied experimentally at Sydney University and Sandia National Laboratories. Turbulence is modeled with a non-linear k-ε type model, taking into account effects of rotation and streamline curvature on the turbulence. Flow and scalar field predictions are in reasonable agreement with experimental data. The influence of the micro-mixing model is small in this case. The mixing model constant C_ϕ has a stronger influence, through the mixture fraction variance. Finite rate chemistry effects are studied in transported scalar PDF calculations using REDIM. For $C_\phi = 2$, a steady solution is obtained with EMST, but with CD the flame extinguishes. The combination REDIM/EMST is not able to predict the local extinction seen in the experiments. Therefore, a final calculation with the CD model with $C_\phi = 3$ is performed and a steady solution is found. With CD, there is more scatter than with EMST, resulting in lower values for temperature and $Y(CO_2)$. Still, this combination REDIM/CD is not able to predict the correct level of local extinction, though.

Introduction

Swirl-stabilized turbulent flames are relevant for many industrial applications, e.g. gas turbines, furnaces, because of their specific advantages compared to non-swirling turbulent flames. The swirling flow in these flames creates recirculation zones which enhance mixing and stabilize the flame. This leads to better combustion efficiency and less pollutant formation. However, swirl flames are quite complex and not yet totally understood.

Several numerical techniques have been used to simulate these complex flows. The unsteady 3D effects are normally better handled by LES than RANS, but LES calculations have a higher computational cost. Therefore, we consider it still useful to study the limitations of RANS and hybrid RANS/PDF calculations in these highly challenging swirling flows, in particular for cases where there is no strong influence from a precessing vortex core (PVC).

A study has already been performed in e.g. [1], but not yet for the Sydney Swirl burner, which was derived from the well-known Sydney bluff-body burner[2]. Experiments have been performed at Sydney University and Sandia National Laboratories [3-7]. The Sydney swirl burner has also been studied numerically by several authors. Masri *et al.* [8] performed a joint velocity-scalar-frequency PDF calculation for a reacting case with the Sydney Bluff Body Burner. LES simulations of non-reacting and reacting cases have been reported by Malalasekera *et al.* [9,10], Stein and Kempf [10,11], El-Asrag and Menon [12] and Olbricht *et al.* [13]

In this study, we show comparable quality results of RANS calculations with the non-linear k-ε model of [14]. The advantage of this 2D axisymmetric approach is that we can also perform transported scalar PDF (probability density function) simulations, in order to study turbulence – chemistry interaction. Finite rate chemistry effects are accounted for by means of a Reaction Diffusion Manifold (REDIM)[15].

We discuss the influence of the micro-mixing model and the model constant C_ϕ on the transported scalar PDF results.

Experimental Set-up

Figure 1 depicts the burner. The bluff body (50mm diameter) contains the central fuel jet (3.6mm diameter). Swirling air is provided through a 5mm wide annulus surrounding the bluff-body. The burner is placed inside a wind tunnel with a square cross section.

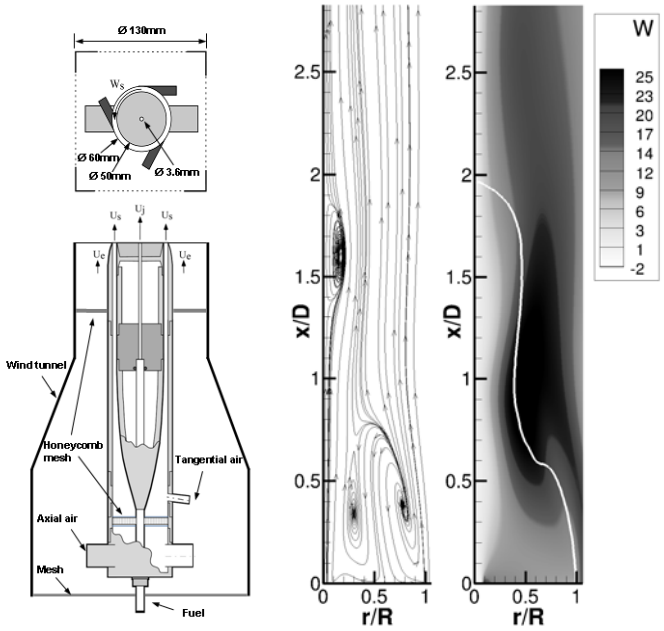

Figure 1: Sydney Swirl Burner (adapted from [16]) and streamlines and tangential velocity from an EMST calculation.

A wide range of testing conditions has been examined experimentally [3-7]. All cases are characterized by: the bulk axial velocity of the central jet (U_j), the bulk axial and tangential velocity of the swirling air annulus (U_s and W_s) and the bulk axial velocity of the co-flow of the wind tunnel (U_e). We consider the swirling flame SM1, where the central jet consists of CH_4. The flow parameters are summarized in table 1. Also reported in this table is the swirl number which is here geometrically defined as $S_g=W_s/U_s$.

Table 1: Flow parameters of SM1.

Case	Fuel	U_e (m/s)	U_j (m/s)	U_s (m/s)	W_s (m/s)	S_g
SM1	CNG/CH4	20	32.7	38.2	19.1	0.5

The flow field of SM1 contains 2 recirculation zones: one close to the bluff body and one further downstream near the central axis. The former is caused by the bluff body, while the latter is caused by vortex breakdown. The recirculation zones are separated by a region of high shear stress which coincides with a highly rotating collar. In [7], this highly rotating collar is believed to be responsible for the vortex breakdown, creating the second recirculation

zone. Local extinction is reported in the region of high shear stress between the two recirculation zones.

Numerical Description and Modeling

All calculations are steady 2D axisymmetric and are performed with the same code PDFD, developed at TU Delft [17]. In the past, PDFD has already successfully been applied to non-swirling cases with the Sydney Bluff Body Burner [17].

The 0.3m long computational domain starts at the burner exit. In radial direction, it is 0.15m wide. A non-uniform rectangular grid of 160x128 cells is used.

Boundary conditions for the inlets were generated based on separate calculations inside the burner. The turbulence levels, however, were far too low, compared to the experimental results close to the burner. Therefore, the profiles of turbulent kinetic energy (k) were scaled up to the level of the experimental values.. The bluff-body was simulated as a slip wall.

The non-linear k-ε turbulence model of [14] is used, as it takes into account the effect of streamline curvature and rotation on turbulence.

The chemistry is modeled with a pre-tabulated REDIM[15]. It can be seen as an extension of the ILDM concept [20] to incorporate the effect of coupling of reaction and diffusion processes. A major advantage of REDIM compared to ILDM is the fact that it also exists in regions where the temperature is low and thus the chemistry is slow.

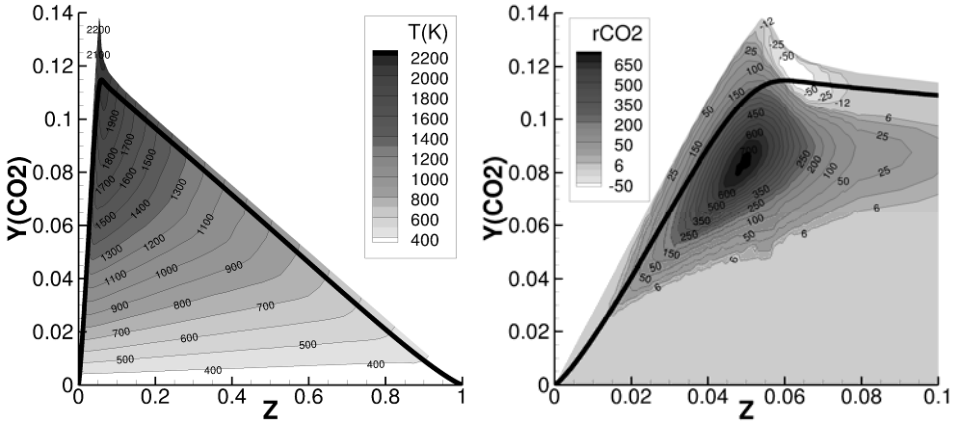

Figure 2: REDIM table for CH_4:
Temperature and reaction rate of CO_2 as a function of mixture fraction and Y(CO_2). Steady diffusion flamelet for a strain rate of $100s^{-1}$ (black line)

More specifically for our case, the REDIM concept was used to reduce the Warnatz mechanism for CH_4 [21] to a 2-dimensional manifold with Z and $Y(CO_2)$ as independent parameters as shown in Figure . Equal diffusivities and unity Lewis number are assumed.

To account for turbulence – chemistry interaction, we use the transported scalar PDF approach. The mass density function $F_\Phi(\psi)=\rho(\psi)\phi_\phi(\psi)$, then obeys the following transport equation [22]:

$$\frac{\partial F_\phi}{\partial t}+\frac{\partial \widetilde{U_j} F_\phi}{\partial x_j}+\frac{\partial}{\partial \psi_\alpha}[S_\alpha(\psi)F_\phi]=-\underbrace{\frac{\partial}{\partial x_j}\left[\left\langle u_j''\middle|\psi\right\rangle F_\phi\right]}_{\text{turbulent diffusion flux}}-\frac{\partial}{\partial \psi_\alpha}\left[\underbrace{\frac{1}{\rho(\psi)}\left\langle\frac{\partial J_j^\alpha}{\partial x_j}\middle|\psi\right\rangle}_{\text{micro-mixing}}F_\phi\right] \qquad (2)$$

In this general equation, S_α is the reaction source term for scalar ϕ_α and $\boldsymbol{J_\alpha}$ the molecular scalar flux. The two terms at the right hand side need to be modeled. For the first term, the turbulent diffusion flux, we apply the gradient diffusion model:

$$-\frac{\partial}{\partial x_j}\left[\left\langle u_j'' \middle| \psi \right\rangle F_\phi\right] = \frac{\partial}{\partial x_j}\left[\Gamma_T \frac{\partial\left(F_\phi/\rho\right)}{\partial x_j}\right] \tag{3}$$

where Γ_T is the turbulent diffusivity, modeled as $\Gamma_T=\mu_T/Sc_T$, with a variable Sc_T [23].

The second term on the right hand side of eq. (3) describes micromixing, which is the molecular diffusion bringing together the reactants necessary for reaction. We will compare two micro-mixing models: the Modified Curl's coalescence/dispersion model (CD) [24] and the Euclidean Minimum Spanning Tree model (EMST) [25-26]. With CD, all particles can interact with each other in a pair-wise manner, while EMST contains a 'localness principle': particles can only interact with particles that are 'close-by' in composition space. In both mixing models the mixing time scale is assumed to be proportional to the integral turbulent length scale:

$$\tau_\phi = \frac{\tau_T}{C_\phi} = \frac{\tilde{k}/\tilde{\varepsilon}}{C_\phi}$$

We use the Lagrangian method to solve eq. (1). Thus, the MDF is represented by a large number of computational particles. The evolution of the particles in physical space is calculated by respectively solving the following differential equation for each of the particles:

$$dX_i^* = (U_i^* + \left[U_i^c\right]^*)dt \tag{4}$$

The superscript * refers to the fact that the value corresponds to a single numerical particle and $[]^*$ are FV properties interpolated at the particle position.

Since we use a scalar PDF, U_i* has to be modeled by the random walk model:

$$U_i^* dt = \left[\tilde{U}_i + \frac{1}{\langle\rho\rangle}\frac{\partial\Gamma_T}{\partial x_i}\right]^* dt + \left[\sqrt{\frac{2\Gamma_T}{\langle\rho\rangle}}\right]^* dW_i \tag{5}$$

The correction velocity U_i^c is calculated with a position correction algorithm[27] and ensures that the volume represented by the particles in a computational cell, equals the cell geometric volume.

The evolution of the particles in composition space is calculated by solving the following differential equation for each of the particles:

$$d\phi_\alpha^* = \theta_\alpha(\varepsilon^*, t)dt + S_\alpha(\phi^*)dt \tag{6}$$

With θ_α the micromixing model and S_α the chemistry term.

The composition vector ϕ consists of mixture fraction and the progress variable $Y(CO_2)$.

Results and Discussion

Transported PDF simulations with REDIM have been performed. For $C_\phi=2$ a steady solution is obtained with EMST , but the flame extinguishes with CD and $C_\phi=3$ is needed to obtain a burning solution. Similar observations were reported in [18] for the non-swirling bluff body flame HM3.

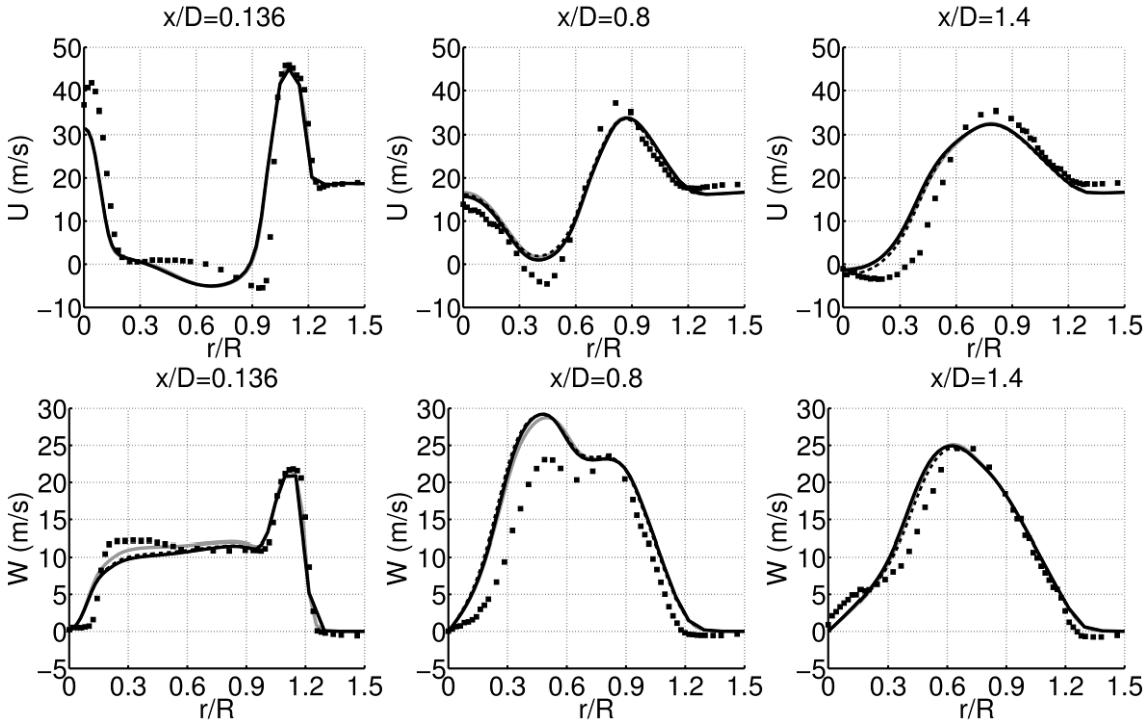

Figure 3: Mean axial and tangential velocity profiles of SM1:
——EMST $\mathbf{C}_\phi$=2 , —— EMST $\mathbf{C}_\phi$=1.5, ····· CD $\mathbf{C}_\phi$=3, ▪ ♦ exp

First we discuss the flow field shown in Figure 3. All calculations have almost identical profiles, suggesting that the micro-mixing model and the mixing constant C_ϕ do not have a substantial influence on the flow field.

At x/D=0.136, all calculations under-predict the mean axial velocity on the centerline. The radial position of the first recirculation zone is not correctly predicted, but the absolute value of the negative velocity is correct. At x/D=0.8, the axial velocity in the center region is slightly over-predicted by all the calculations. The calculations show no negative axial velocities. In the experiments, however, a wide area of negative velocities is observed, indicating the length of the first recirculation zone is under-predicted by all calculations. For all calculations, the width of the recirculation zone is smaller than in the experiments, but the axial position of the beginning of the second recirculation zone is reasonably predicted. The predictions of the mean tangential velocity W are also satisfactory. At x/D=0.136, the sharp gradient around r/R=0.15 could not be captured by any of the calculations. At x/D=0.8, with all calculations over-predict the experimental mean tangential velocity. Further downstream all the calculations correctly predict the tangential velocity. Note that, in general, agreement with experimental data is quite good, comparable to what was obtained with LES [10]

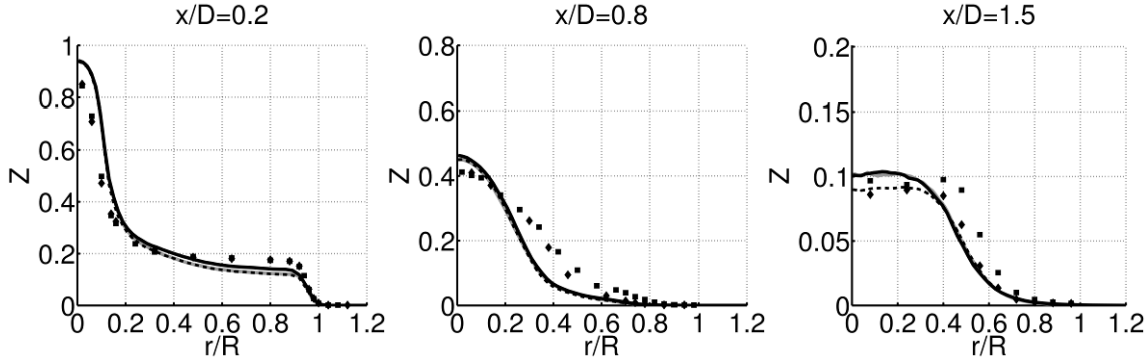

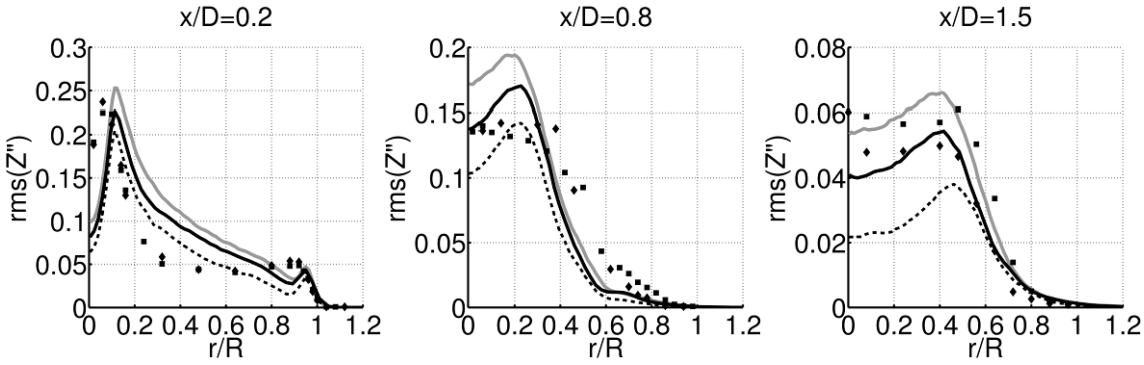

Figure 4: Mean mixture fraction and mixture fraction rms profiles of SM1:
——EMST $\mathbf{C_\phi}$=2 , —— EMST $\mathbf{C_\phi}$=1.5, ····· CD $\mathbf{C_\phi}$=3, ▪ ♦ exp

Next we discuss the composition fields, starting with the mean mixture fraction and mixture fraction rms profiles shown in figure 3.

At x/D=0.2, the good predictions of the mean mixture fraction were obtained due to the use of the variable Sc_T [] close to the bluff body. All calculations have almost identical profiles, but the EMST calculation with C_ϕ=*1.5* and the CD calculation have a slightly lower mean mixture fraction in the bluff body region. All calculations under-predict the mixture fraction rms in the center region and over predict it in the bluff body region. Contrary to the mean mixture fraction the mixture fraction rms profiles of the different calculations differ substantially, with higher rms values for lower C_ϕ values. This is as expected, as lower C_ϕ values correspond to a slower decay of the scalar fluctuations. At x/D=0.8, the mean mixture fraction profiles are even more identical for all calculations and they are steeper compared to the experimental profile suggesting the calculations under-predict turbulent mixing of mass. The mixture fraction rms profiles, differ now the most in the center region, again with higher rms values corresponding with lower C_ϕ values. At x/D=1.5, the CD calculation correctly predicts the mean mixture fraction in the center region while the EMST calculations slightly over-predict it. The CD calculation however under-predicts the mixture fraction rms due to the high C_ϕ value, while the lower C_ϕ values of the EMST calculations lead to better results.

In general, the influence of the micro-mixing model on the mean mixture fraction only becomes important at a substantial distance from the burner. The mean mixture fraction rms on the other hand is mainly influenced by C_ϕ .

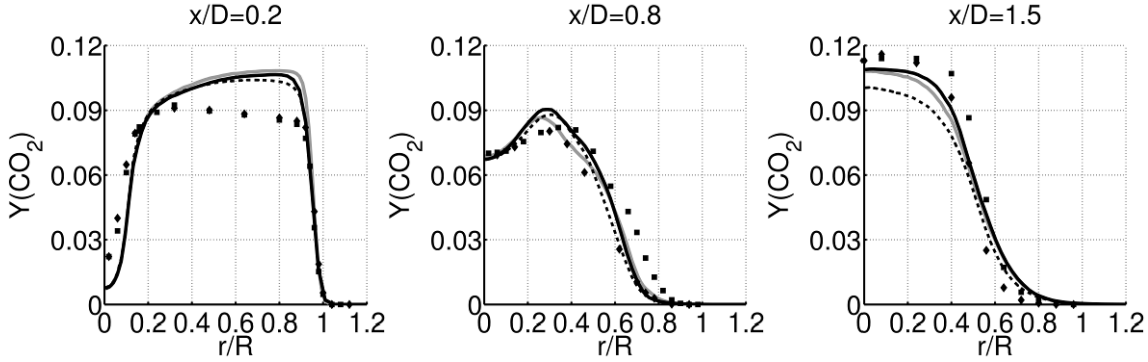

Figure 5: $Y(CO_2)$ profiles of SM1: see Fig. 6

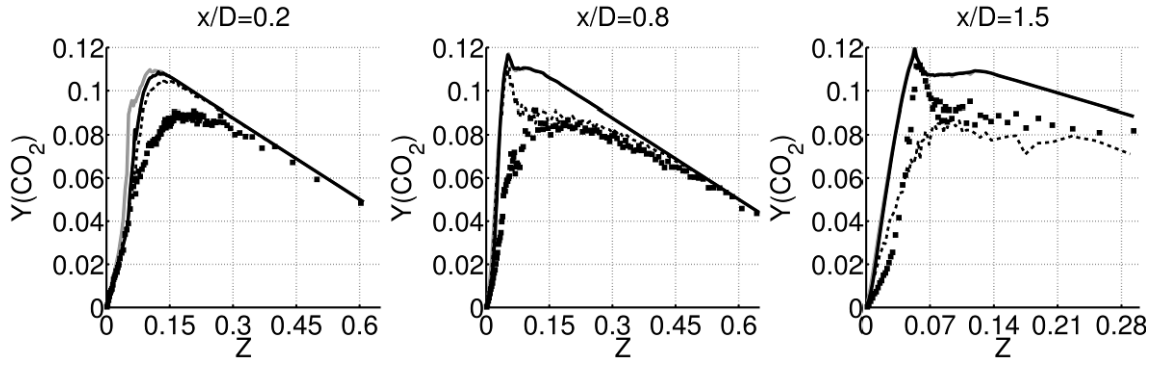

Figure 6: Conditional $Y(CO_2)$ profiles of SM1:see Fig. 3

The mean profiles of *Y(CO₂)*, the second independent parameter of the REDIM table, are shown in figure 5. At x/D=0.2, all the calculations over-predict *Y(CO₂)* in the bluff body region due to the under-prediction of the mean mixture fraction in that region and due to the over-prediction of the conditional mean *Y(CO₂)* for Z=0.06-0.4. In the center region, on the other hand, all calculations under-predict the mean *Y(CO₂)* only due to the over-prediction of *Z.* The profiles of the calculations slightly differ among each other mainly due to differences in mean mixture fraction and conditional mean *Y(CO₂)*. At x/D=0.8, all calculations give very good predictions of the mean *Y(CO₂)*, even though the mean mixture fraction was not predicted well at this axial position. The EMST calculations over-predict the conditional mean of *Y(CO₂)* for Z<0.5, while the CD calculation only over-predict the conditional mean of *Y(CO₂)* for Z<0.15. Nonetheless, the mean *Y(CO₂)* profiles of the EMST calculation with C_ϕ=2 and the CD calculation do not differ that much (Fig. 5). At x/D=1.5, the EMST calculations slightly under-predict the mean *Y(CO₂)* in the center region while the CD calculations predict even lower values, due to the lower conditional mean of *Y(CO₂)* counteracting the lower mean mixture fraction for the CD calculations in that region. This higher conditional mean of the mean *Y(CO₂)* for CD indicates there is more scatter in *Y(CO₂)*-space compared to the EMST calculations even though there is less scatter in Z-space (Figure 4). This is confirmed by the scatter plots shown in figure 7.

In general the influence of the mixing model of the mean and conditional mean *Y(CO₂)* becomes more important further downstream. The mixing constant C_ϕ, on the other hand, only influences the conditional mean *Y(CO₂)* close to the bluff body. The mean *Y(CO₂)* predictions are influenced indirectly by C_ϕ, through the changed mixture fraction rms.

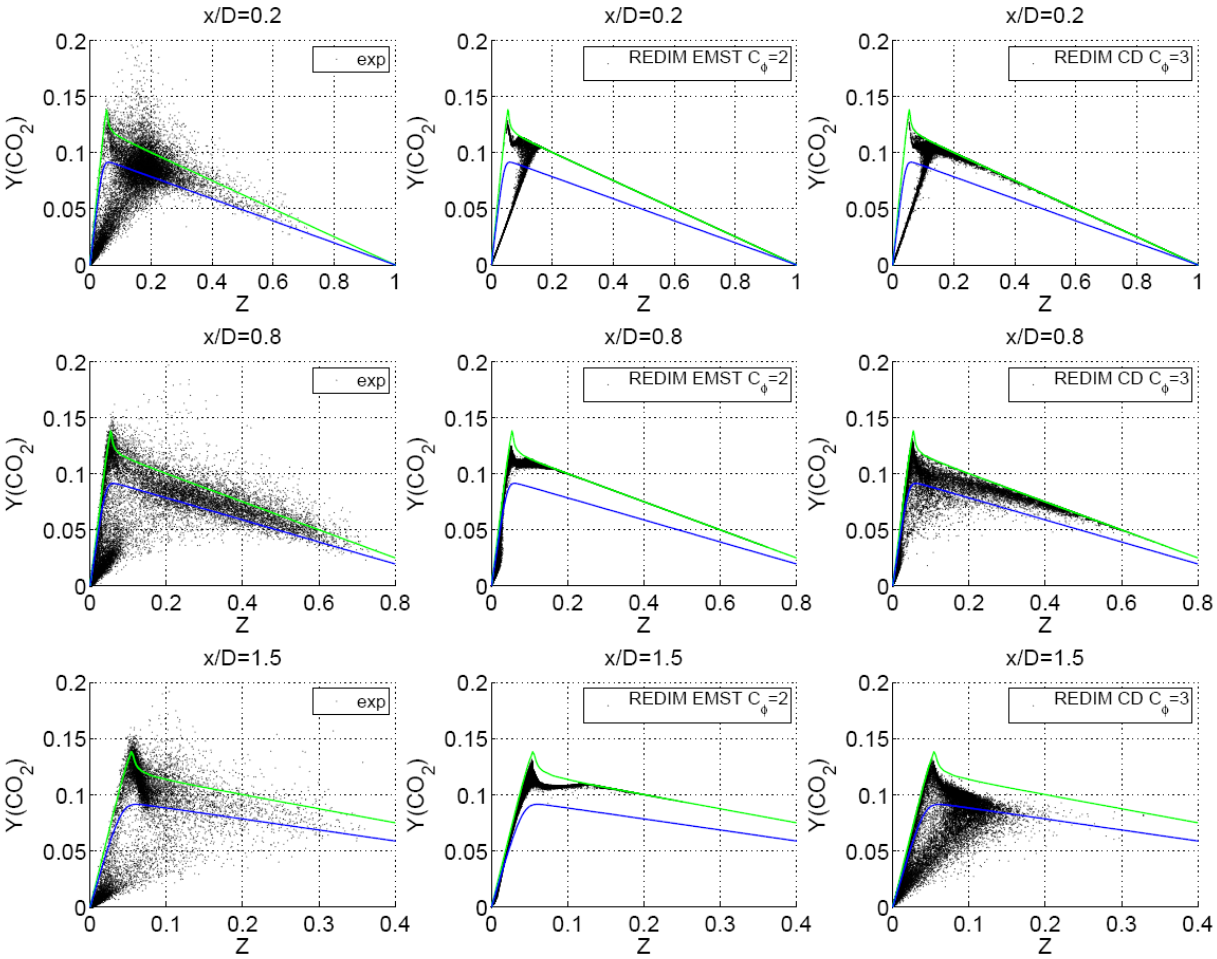

Figure 7: Scatter plot of $Y(CO_2)$:
upper boundary of REDIM(green line), steady diffusion flamelet close to extinction (blue line)

Now we analyse more closely the scatter plots of *$Y(CO_2)$* shown in figure 7. The green line is the upper boundary of the REDIM and the blue line is a steady diffusion flamelet close to extinction. At x/D=0.2, the scatter plots of the calculations are very similar, with slightly more scatter for the CD calculations. The line like structure, connecting the origin with the rich flamelet branch, is a mixing line representing mixing of combustion products with unburnt gasses as discussed in [23]. Also the points in the experimental scatter plots are clustered around a mixing line indicating a large part of the scatters in this region are due to mixing, although the scatters deviating from the mixing line might be due to extinction. At x/D=0.8, the scatter plots of the calculations differ substantially. The computational particles of the EMST calculation only access a confined space similar to a flamelet structure. The CD calculation on the other hand shows more scatter and accesses a larger area in composition space. Still, the level of scatter as observed in the experiments is not obtained. At this axial location, the majority of the points in the experimental scatter plots are likely due to local extinction. At x/D=1.5, the scatter plot of the EMST calculation still resembles a flamelet. The scatter plot contains a substantial amount of scatter, but the distribution of the points in composition space is different from that in the experimental scatter plot as is also reflected in the conditional mean. Again a mixing line structure is observed in the scatter plot of the CD calculation, but now with more scatter around mixing line. This is due to mixing of unburnt gasses with combustion products from the second recirculation zone. This mixing line structure can not be easily observed in the experimental scatter plots, where again local extinction is most likely the cause for the observed scatter.

In general, the amount of scatter for CD is substantially higher than for EMST and the difference is larger further downstream. This is due the localness property. With CD, all particles can interact with each other (non-localness), while with EMST only particles which are close in composition space will interact (localness).

We analyse the behaviour of the mixing models more profoundly by following the computational particles as they move through composition space.

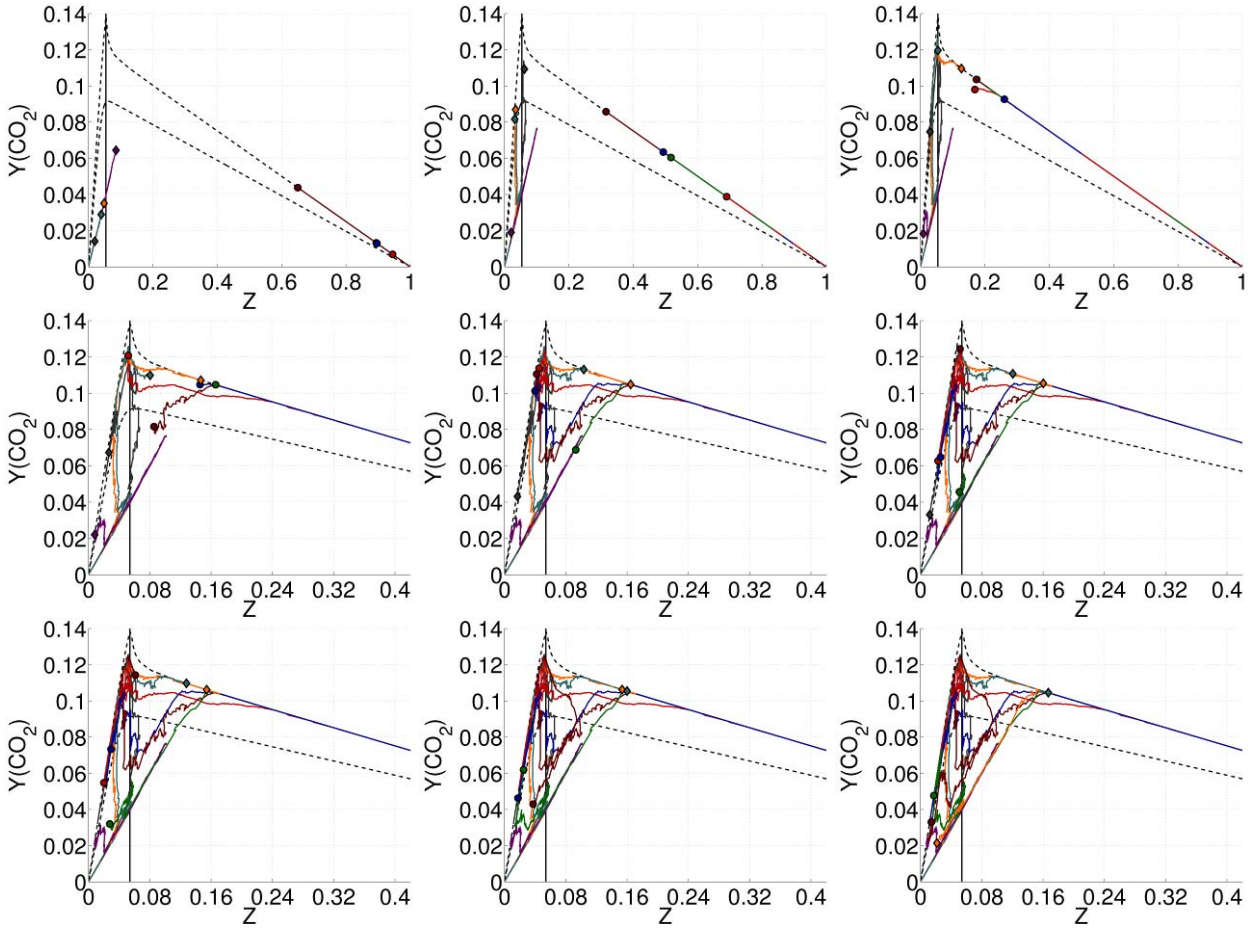

Figure 8: Evolution of representative computational particles for EMST calculation with C_ϕ=2 :
particles injected at the fuel inlet (diamonds), particles inject at annulus air inlet (circle) upper boundary of the REDIM (upper dashed line), steady diffusion flamelet close to extinction(lower dashed line), stoichiometric mixture fraction (vertical black line)

In figure the evolution of some representative tracers from the EMST-calculation with C_ϕ =2 are shown. The particles injected at the annulus either move along the lean flamelet branch or the flatter mixing line, as seen in the eulerian scatter plots at x/D=0.2. The particles injected at the fuel jet first follow the rich flamelet branch before reacting or mixing with leaner, less reactive gases, resulting in the mixing line structure seen in the scatter plots at x/D=0.2

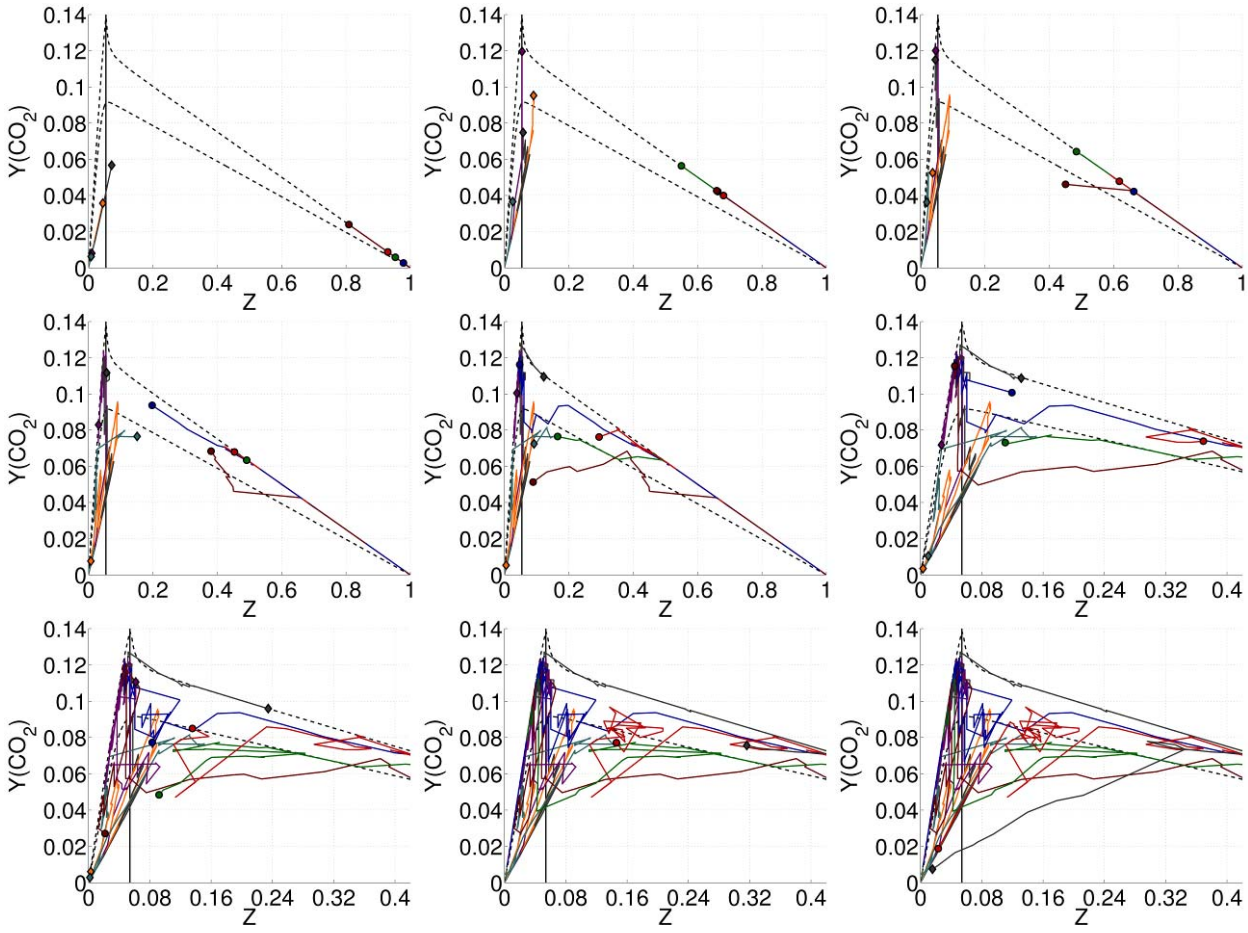

Figure 9: Evolution of representative computational particles for CD calculation with C_{ϕ}=3 : particles injected at the fuel inlet (diamonds), particles inject at annulus air inlet (circle) upper boundary of the REDIM (upper dashed line), steady diffusion flamelet close to extinction(lower dashed line), stoichiometric mixture fraction (vertical black line)

The tracers of the CD calculations shown in figure are harder to follow as they jump in composition space due to the non-localness of CD. This also leads to the higher amount of scatter observed in the eulerian scatter plots. The tracers injected at the fuel inlet can jump of the rich flamelet branch at richer mixture fraction than is the case with the EMST model. Therefore lower $Y(CO_2)$ values are reached for $Z=Z_{stoich}-0.4$ as seen in the scatter plots of CD at x/D=0.8 and 1.5. Due to non-localness air can mix with a larger range of compositions on the rich flamelet branch leading to mixing lines different from the one observed for both mixing models at x/D=0.2. This is confirmed by th mixing line like trajectory of the gray tracer from the rich flamelet branch in Figure 9.

In the framework of EMST calculations none of the mixing models are able to correctly model local extinction. EMST under-predicts the amount of scatter. CD on the other hand predicts a reasonable amount of scatter, which might be interpreted as local extinction in the scatter plots, but this is rather a consequence of the non-localness allowing mixing of unburnt lean and mix particles through the reaction zone, as the Lagrangian tracers showed. To model local extinction the fluctuations of the scalar dissipation rate need to be represented and this is not the case for this modeling framework, as a mean mixing time scale is used within one cell.

However, it is not clear whether we observe here a weakness of the mixing models, or whether the use of the mixing model highlights other limitations in the modelling: limitations of REDIM in order to model local extinction, limitations of the velocity-scalar correlation

modelling (i.e. the use of joint scalar PDF modelling instead of joint velocity-scalar PDF), or even limitations of the RANS approach for this flame where unsteady effects in physical space may have a strong impact on the results in composition space.

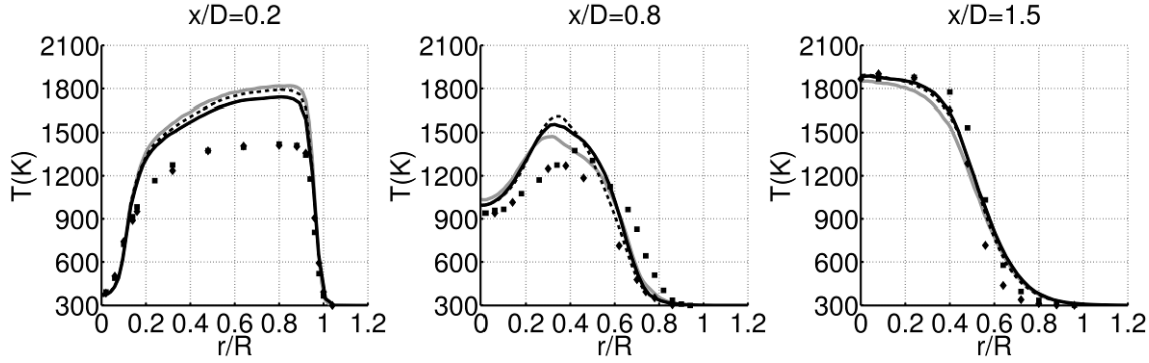

Figure 7: *Temperature profiles of SM1: see Fig. 6*

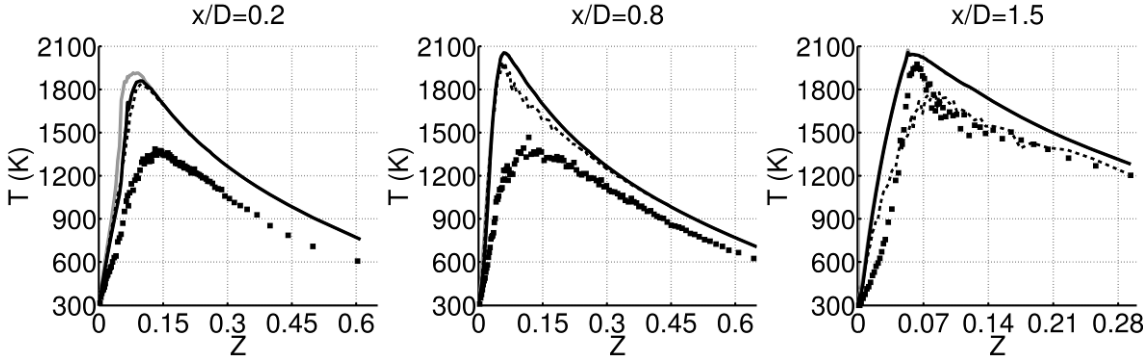

Figure 8: *Conditional temperature profiles of SM1:*

Although both $Y(CO_2)$ and temperature are measures of reaction progress, the mean profiles differ. For example, while the CD calculations predict lower values of $Y(CO_2)$ compared to the EMST calculation with C_ϕ=2, the temperature in the is higher than that of the EMST calculation with C_ϕ=2. This is due to the smaller difference in the conditional mean of temperature(Figure 8) for both calculations, compared to the conditional mean of $Y(CO_2)$. Therefore the lower mean mixture fraction value of the CD calculation is now not counteracted by the lower conditional mean of temperature, which was the case for $Y(CO_2)$. In general the conditional mean of temperature is over-predicted more strongly than the conditional mean of $Y(CO_2)$. At x/D=0.2 and x/D=0.8 this leads to a stronger over-prediction of the mean temperature. At x/D=1.5, on the other hand, this results in a correct prediction of the mean temperature for all calculations.

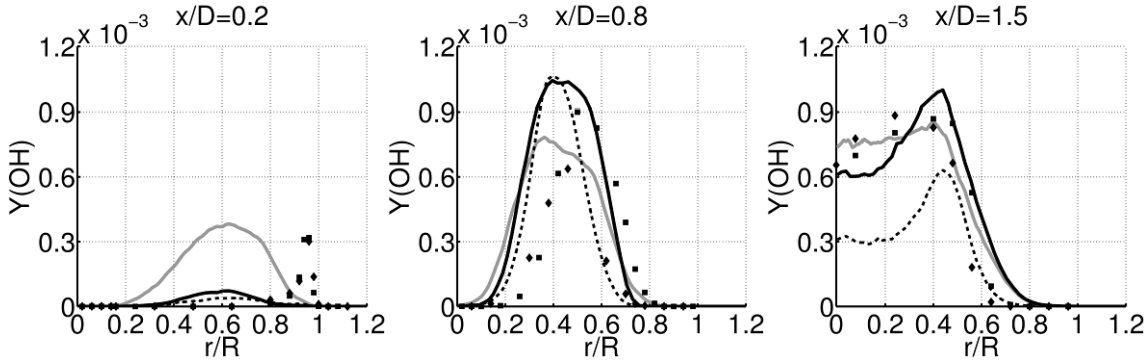

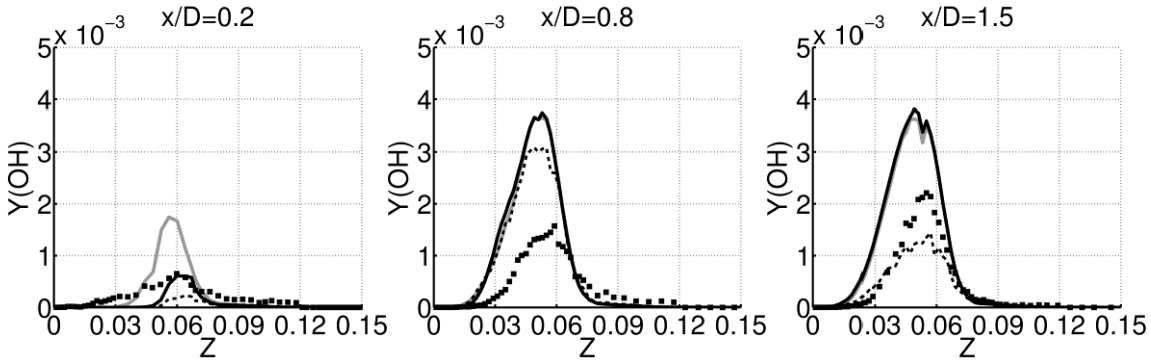

Finally, the mean (figure) and conditional mean of *Y(OH)* are discussed. In general the mean Y(OH)-profiles for the different calculations differ strongly due to the different prediction of the mean mixture fraction close to stoichiometry and the different conditional means of Y(OH). As for temperature, the conditional means of Y(OH) for the EMST with different values of C_ϕ only differ close to the bluff body, where the calculation with C_ϕ=2 gives the best prediction.. Further downstream, the EMST calculation systematically over-predicts the conditional mean of Y(OH) due to the under-prediction of the amount of scatter in Y(OH)-space, resulting from an under-prediction of the amount of scatter in $Y(CO_2)$-space. The CD calculation on the other hand has more scatter in $Y(CO_2)$ and Y(OH)–space, resulting in lower conditional means of Y(OH).

Conclusions

Steady 2D axisymmetric hybrid RANS-PDF calculations with a non-linear k-ε model were performed for a reacting swirling flow behind a bluff-body burner. Finite rate chemistry effects were studied with transported scalar PDF calculations using the REDIM model. For $C_\phi = 2$, a steady solution is obtained with the EMST model, but with the CD model a value of $C_\phi = 3$ was needed to obtain a burning solution. The turbulent flow and composition field predictions are in good agreement with experimental data. The influence of the micro-mixing model on the results in physical space is small, but becomes more important further downstream. The influence of the micro-mixing model is observed more clearly, where the larger fluctuations in $Y(CO_2)$-space for the CD model lead to lower conditional means. This effect is again stronger further downstream.. The mixing constant C_ϕ influences the results in physical space, through the mixture fraction variance. Its influence in composition space on the other hand is only visible close to the bluff body. Using EMST, the local extinction seen in the experiments cannot be predicted.. The steady CD solution leads to a higher amount of scatter than with EMST, resulting in lower values for temperature and $Y(CO_2)$. However, using CD and C_ϕ=3, local extinction is still not correctly predicted.

Acknowledgements

This work is funded by the Special Research Fund of Ghent University under project BOF07/DOC/210 and is also supported by the Comunidad de Madrid through Project HYSYCOMB, P2009/ENE-1597 and by the Spanish Ministry of Science and Innovation under Project ENE2008-06515-C04-02.

Nomenclature

C_ϕ	mixing constant
D	diameter of the bluff body
k	turbulent kinetic energy
F_ϕ	scalar mass density function
$F(\Phi)$	vector of chemical source terms

J_α	molecular scalar flux
r	radial coordinate
R	radius off the bluff body
T	temperature
x	axial coordinate
S_g	swirl number
S_α	reaction source term
Sc_T	turbulent Schmidt number
$u''v''$	shear stress
U_j	axial velocity of the fuel jet
U_s	axial velocity of the annulus
U_e	axial velocity of the coflow
U_i^c	correction velocity
W_s	tangential velocity of the annulus
dW_i	derivative of the Wiener process
$Y(N_2)$	mass fraction of N_2
$Y(CO_2)$	mass fraction of CO_2
Γ_T	turbulent diffusivity
ε	turbulent dissipation rate
ϕ	composition vector
Φ	thermo-kinetic state vector
Φ_ϕ	the matrix of partial derivatives of Φ with respect to ϕ
$\Phi_{\phi_i\phi_j}$	second partial derivatives of Φ with respect to ϕ_I and ϕ_j
θ_α	micromixing model
ρ	density, d the diffusion coefficient,
ϖ_i	estimates for the spatial gradients of the reduced coordinates.
μ_T	turbulent viscosity
Z	mixture fraction

References

[1] Wegner, Maltsev, Schneider, Sadiki, Dreizler, Janicka, "Assessment of unsteady RANS in predicting swirl flow instability based on LES and Experiments", *Int. Journal of Heat and Fluid Flow 25*, 528-536 (2004)

[2] Dally, B., Masri, A., Barlow, R. and Fiechtner, G., "Instantaneous and Mean Compositional Structure of Bluff-Body Stabilized Nonpremixed Flames ", *Comb. and Flame* 114 119-148. (1998)

[3] Al-Abdeli, Y.M. and Masri, A.R., "Recirculation and flowfield regimes of unconfined non-reacting swirling flows", *Experimental Thermal and Fluid Science* 27 655-665 (2003).

[4] Kalt, P., Al-Abdeli, Y., Masri, A and Barlow, R, "Swirling turbulent non-premixed flames of methane: Flow field and compositional structure", *Proc. Comb. Inst.* 29 1913-1919. (2002)

[5] Masri, A.R., Kalt, P.A.M. and Barlow, R.S., "The compositional structure of swirl-stabilised turbulent nonpremixed flames", *Comb.and Flame* 137 1-37 (2004).

[6] Y.A.Al-Abdeli, Masri, A.R., Marquez, G.R. and Starner, S.H., "Time-varying behaviour of turbulent swirling nonpremixed flames", *Comb. and Flame* 146 200-214 (2006).

[7] Masri, A, Kalt, P., Al-Abdeli, Y.M. and Barlow, R.S., "Turbulence-chemistry interactions in non-premixed swirling flames", *Comb. Theory and Mod.* 11 653-673 (2007).

[8] Masri, A., Pope, S. and Dally, B., "Probability density function computations of a strongly swirling nonpremixed flame stabilized on a new burner", *Proc. Comb. Inst.* 28 123-131(2000).

[9] Malalasekera, W., Ranga-Dinesh, K., Ibrahim; S. and Masri, A.R., "LES of Recirculation and Vortex Breakdown in Swirling Flames", *Comb. Sci. and Tech.* 180 809-832(2008).

[10]Kempf, A., Malalasekera, W., Ranga-Dinesh, K.K.J. and Stein, O., "Large Eddy Simulations of Swirling Non-premixed Flames With Flamelet Models: A Comparison of Numerical Methods", *Flow Turb. and Comb.*81 523-561(2008).

[11]Stein, O. and Kempf, A., "LES of the Sydney swirl flame series: a study of vortex breakdown in isothermal and reacting flows", *Proc. Comb. Inst.* 31 1755-1763(2007).

[12]El-Asrag, H. and Menon, S., "Large eddy simulation of bluff-body stabilized swirling non-premixed flames", *Proc. Comb. Inst.* 31 1747-1754(2007).

[13]Olbricht, C., Ketelheun, A., Hahn, F., Janicka, J., "Assessing the Predictive Capabilities of Combustion LES as Applied to the Sydney Flame Series", *Flow Turb. and Comb*.85 513-547 (2010)

[14]Merci, B. and Dick, E., "Heat transfer predictions with a cubic k-epsilon model for axisymmetric turbulent jets impinging onto a flat plate", *Int. J. of Heat and Mass Transfer* 46 469-480(2003).

[15]Bykov, V., Maas, U., "The extension of the ILDM concept to reaction-diffusion manifolds", *Comb. Theory and Mod.* 11 839–862(2007).

[16]http://www.aeromech.usyd.edu.au/thermofluids/swirl_files/burner-plan.pdf

[17]Naud, B., Jimenez, C., Roekaerts, D., "A consistent hybrid PDF method: implementation details and application to the simulation of a bluff-body stabilised flame", *Prog. in Comp. Fluid Dyn.*6 (1-3) 146-157 (2006)

[18]Merci, B., Roekaerts, D., Naud,**,** B. and Pope, S.B., "Comparative study of micromixing models in transported scalar PDF simulations of turbulent nonpremixed bluff body flames", *Comb. and Flame* 146 109-130(2006)

[19]Lutz, A.E., Kee, R.J., Grcar, J.F.,. Rupley, F.M, Technical Report SAND96-8243, UC-1409, Sandia National Laboratories (1996).

[20]Maas, U., Pope, S.B., "Simplifying Chemical Kinetics – Intrinsic low-dimensional manifolds in composition Space", *Comb. and Flame* 88 (3-4) 239-264 (1992)

[21]Warnatz J., Maas, U., Dibble R, *Combustion: Physical and Chemical Fundamentals, Modeling and Simulation, Experiments, Pollutant Formation,* 2nd edition, Springer,1999,96

[22]Pope, S.B.," Pdf methods for turbulent reactive flows", *Progress in Energy and Combustion Science* 11 119-192 (1985).

[23]R.De Meester, B.Naud, U.Maas and B.Merci, Transported scalar PDF calculations of a swirling bluff body flame (`SM1') PART 1: Influence of the use of a progress variable in the chemistry model, *Comb. and Flame,* submitted

[24]Janicka, J., Kolbe W., Kollman, W., "Closure of the transport-equation for the probability density function of turbulent scalar fields", *J. Non-Equil. Thermodyn*.4 47–66(1979).

[25]Subramaniam, S., S.B. Pope, "A mixing model for turbulent reactive flows based on Euclidean minimum spanning trees", *Comb.and Flame* 115 487–514(1998).

[26]Subramaniam, S., Pope; S.B., "Comparison of mixing model performance for nonpremixed turbulent reactive flow", *Comb. and Flame* 117 (4) 732–754 (1999).

[27] Muradoglu, M., Liu, K. and Pope, S.B. "PDF modeling of a bluff-body stabilized turbulent flame", *Comb. and Flame,* 132, . 115–137 (2003)